APL Photonics

Perfectly absorbing dielectric metasurfaces for photodetection

Cite as: APL Photonics **5**, 101304 (2020); https://doi.org/10.1063/5.0019883
Submitted: 25 June 2020 . Accepted: 25 September 2020 . Published Online: 20 October 2020

Oleg Mitrofanov, Lucy L. Hale, Polina P. Vabishchevich, Ting Shan Luk, Sadhvikas J. Addamane, John L. Reno, and Igal Brener

Perfectly absorbing dielectric metasurfaces for photodetection

Cite as: APL Photon. 5, 101304 (2020); doi: 10.1063/5.0019883
Submitted: 25 June 2020 • Accepted: 25 September 2020 •
Published Online: 20 October 2020

Oleg Mitrofanov,[1,2,a)] Lucy L. Hale,[1] Polina P. Vabishchevich,[2,3] Ting Shan Luk,[2,3] Sadhvikas J. Addamane,[2,3] John L. Reno,[2,3] and Igal Brener[2,3]

AFFILIATIONS

[1] University College London, Electronic and Electrical Engineering, London WC1E 7JE, United Kingdom
[2] Center for Integrated Nanotechnologies, Sandia National Laboratories, Albuquerque, New Mexico 87123, USA
[3] Sandia National Laboratories, Albuquerque, New Mexico 87185, USA

[a)] **Author to whom correspondence should be addressed:** o.mitrofanov@ucl.ac.uk

ABSTRACT

Perfect absorption of light by an optically thin metasurface is among several remarkable optical functionalities enabled by nanophotonics. This functionality can be introduced into optoelectronic devices by structuring an active semiconductor-based element as a perfectly absorbing all-dielectric metasurface, leading to improved optical properties while simultaneously providing electrical conductivity. However, a delicate combination of geometrical and material parameters is required for perfect absorption, and currently, no general all-dielectric metasurface design fulfills these conditions for a desired semiconductor and operation wavelength. Here, using numerical simulations, we demonstrate that Mie resonators with subwavelength-size interconnecting channels allow this combination of perfect absorption requirements to be satisfied for different wavelengths of operation and different levels of intrinsic material absorption. We reveal the underlying physics and show that interconnecting channels play a critical role in achieving perfect absorption through their effects on the resonant wavelengths and losses for the electric dipole and magnetic dipole modes in Mie resonators. By adjusting only the channel widths, perfect absorption can be achieved for an optically thin GaAs-based metasurface at a desired wavelength of operation in a range from 715 nm to 840 nm, where the intrinsic absorption level in GaAs varies by more than a factor of 2. Optical transmission experiments confirm that these metasurfaces resonantly enhance optical absorption. This work lays out the foundation and guidelines for replacing bulk semiconductors with electrically connected, optically thin, perfectly absorbing metasurfaces in optical detectors.

I. INTRODUCTION

Optical metasufaces have enabled remarkable functionalities and devices,[1–5] including flat optical components that replace three-dimensional counterparts[6,7] and schemes for controlling light directionality in refraction and scattering.[8,9] Parallel to these developments, plasmonic and, more recently, all-dielectric metasurfaces exhibiting enhanced light absorption have been proposed and used to improve solar cells and various types of photodetectors,[10–17] where performance correlates with absorption enhancement as well as with the reduced thickness of the active region.[16,17] Ultimate enhancement of absorption in a very thin layer can be achieved using perfect absorber configurations,[18,19] such as impedance matched ultra-thin dielectric layers,[20] arrays of plasmonic resonators,[21–25] and photonic crystal structures.[26–28] In addition to those approaches, arrays of all-dielectric nanoscale resonators[17,29–31] are particularly attractive for optoelectronic devices since the active semiconductor-based element can be structured as an all-dielectric metasurface with desired optical as well as electronic properties, combining different metasurface-enabled functionalities in one structure. For example, all-dielectric perfectly absorbing metasurfaces were used to replace the photoconductive element to improve the efficiency of terahertz detectors by an order of magnitude.[32]

Despite the promising potential for improving the performance of optoelectronic devices, all-dielectric perfectly absorbing metasurfaces have not yet been exploited widely. Slow adaptation of this

approach can be attributed to two challenges. First of all, a delicate combination of conditions is required for the perfect absorption effect to occur. For a metasurface consisting of dielectric resonators, it needs to support two modes of opposite symmetry at the wavelength of operation,[29–32] and these two modes need to be critically coupled to the incident wave.[33,34] Second, the metasurface needs to support charge carrier conduction so that photoexcited carriers can be collected at the device electrodes. Currently, there is no general design fulfilling all of the above-mentioned conditions for a desired device architecture, semiconducting material, or device operation wavelength.

One route to realizing perfect absorption is to use two Mie modes in dielectric resonators,[35] such as the in-plane and out-of-plane magnetic dipole (MD) modes,[17] or a combination of an in-plane MD and an in-plane electric dipole (ED) mode.[29,30] While the out-of-plane modes require special designs for their excitation,[17] the in-plane modes couple directly to the incident light. The in-plane MD and ED modes of a symmetric Mie resonator also display the opposite symmetries—satisfying the symmetry requirement mentioned before. However, these modes generally occur at different wavelengths. The required mode degeneracy, also known as the Kerker condition[36] used in Huygens sources, has been achieved with special geometrical shapes, for example, cylinders,[9,29,30] by using electromagnetic coupling between adjacent resonators,[9,37–40] and using a continuous Mie-resonant membrane metasurface.[41]

However, in addition to the degeneracy, the ED and MD modes must be critically coupled to the incident excitation, i.e., the mode radiative losses must be equal to the mode intrinsic losses.[33,34] Satisfying this requirement for a desired material and desired wavelength operation is not always possible.[34] Furthermore, to enable electrical conduction, the metasurface must include interconnecting channels, which may affect the resonator mode wavelengths and destroy degeneracy.

Here, we demonstrate that the subwavelength-size interconnecting channels can be used to solve these challenges. The channels provide the means for the effective adjustment of the critical coupling condition for different wavelengths of operation and different levels of intrinsic material absorption while enabling electronic conductivity within the metasurface. We reveal the underlying physics using numerical simulations and describe how the channels affect the condition of critical coupling and the wavelength at which perfect absorption occurs. By adjusting only the size of interconnecting channels, perfect absorption in a GaAs resonator-based metasurface can be achieved for a desired wavelength in a range from 715 nm to 840 nm. We emphasize that despite a change in intrinsic absorption within this range by more than a factor of 2, which upsets the delicate balance of radiative and intrinsic losses required by the critical coupling condition, the proposed metasurface architecture allows us not only to change the position of the resonances but also to restore that balance and achieve perfect absorption at a desired wavelength. We experimentally verify that the proposed design exhibits strong resonant absorption. Although the operation principle is not broadband due to reliance on the resonant Mie mode excitation, metasurfaces made of GaAs provide an absorption band of ~50 nm, sufficiently wide for many practical applications. This work lays out the foundation for a new class of more efficient and more compact photodetectors, where bulk semiconductor elements are replaced with optically thin perfectly absorbing metasurfaces. For example, this design can be used to improve the efficiency and performance of photoconductive switches for terahertz pulse detection[32] and PIN photodiodes for telecommunication applications.

II. RESULTS AND DISCUSSION

A. Metasurface design

We use a commercial finite difference time domain electromagnetic solver[42] to numerically model optical properties. For metasurface material, we use GaAs wavelength-dependent parameters (Palik model). We also use fixed values of n and κ to illustrate the effect of geometry where stated. A single unit cell is simulated with periodic x- and y-boundaries and perfectly matched layer (PML) boundaries in the z-direction. For modeling the substrate, a constant refractive index, no loss dielectric material ($n = 1.57$) is used below and between the resonators, and $n = 1$ representing air is used above the metasurfaces. The metasurface is illuminated from the substrate side at normal incidence by a y-polarized plane wave (to ensure the excitation of the desired modes: a MD with the magnetic field vector in the x-direction, M_x, and an ED with the electric field vector in the y-direction, E_y). Absorbed power $A(\lambda)$ is calculated as a product of the electric field intensity and the imaginary part of the permittivity, integrated over the unit cell and normalized to the incident power. The accuracy of the calculations is verified using simulated reflectivity $R(\lambda)$ and transmission spectra $T(\lambda)$ as $A = 1 - (R + T)$.

To achieve perfect absorption in a metasurface consisting of interconnected semiconductor resonators, we begin our design with an array of cubic GaAs resonators and find their MD and ED modes. We select cubes of size $a = 160$ nm, arranged in a uniform square lattice with periods $P_x = P_y = 320$ nm. Using numerical simulations, we identify the MD and ED modes, which are centered at different wavelengths, more than 100 nm apart, at 694 nm and 590 nm, respectively [Fig. 1(a)]. We then transform the cubes into rectangular resonators to bring the two modes into degeneracy. This is achieved by elongating the cube along one axis orthogonal to the polarization of incident light and the incident wavevector. This transformation shifts the ED mode with the electric field vector oriented along the y-axis to a longer wavelength while keeping the MD mode at approximately the same wavelength, as explained in the supplementary material. In addition, we introduce parallel channels along the y-axis connecting the resonators into a network, which enables charge conduction, as illustrated in Fig. 1(b).

To verify that the above-described geometrical transformation leads to the degeneracy of the MD and ED modes, we numerically simulate absorption in the metasurfaces shown in Figs. 1(a) and 1(b). To quantify the transformation, we introduce a parameter, L, equal to the ratio of the resonator size in the x-direction W_x to the lattice period P_x: $L = W_x/P_x$ [Fig. 1(c)]. We link this parameter to the width of the conduction channel w_x as $w_x = (L - 0.5) \cdot a$ so that the channel is introduced gradually in small increments. As a result, this parameter conveniently describes different cases of the metasurface: $L = 0.5$ represents the array of cubic resonators [Fig. 1(a)], and $0.5 < L < 1$ represents the arrays of interconnected rectangular resonators with the channel width ranging from 0 nm to 80 nm. A

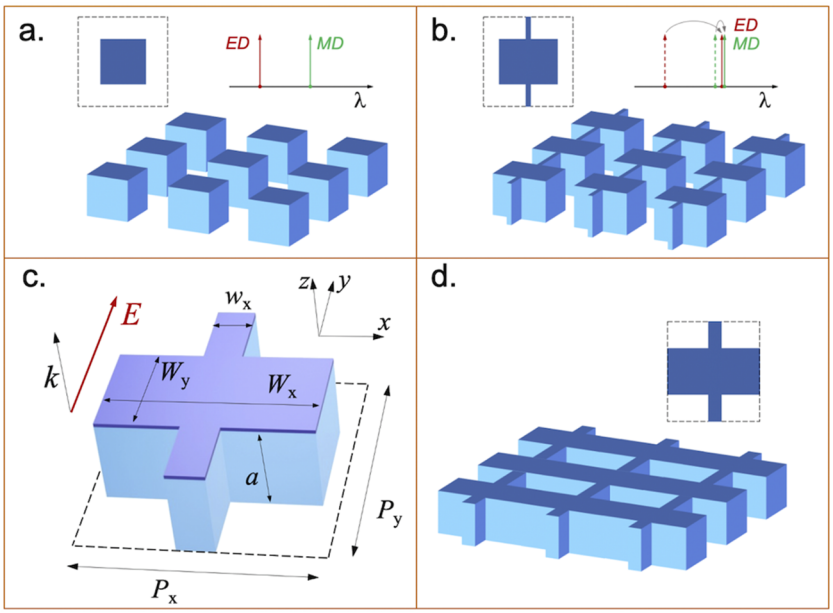

FIG. 1. Design of the perfectly absorbing metasurface. (a) A reference metasurface consisting of cubic resonators in a square lattice, where the two lowest order Mie modes (MD and ED) occur at different wavelengths. (b) Metasurface consisting of interconnected rectangular resonators, where the ED and MD mode wavelengths overlap. (c) Schematic diagram of the metasurface unit cell showing the dielectric resonator dimensions. (d) A special case of the perfectly absorbing metasurface with $L = W_x/P_x = 1$.

special case $L = 1$ represents a metasurface with resonators joined into continuous bars along the x-axis with 80 nm wide channels along the y-axis [Fig. 1(d)]. This gradual transformation described by parameter L allows us to track the resonant wavelengths of the ED and MD modes for different cases.

First, we use a simplified material model to resolve modes supported by the metasurface clearly and to eliminate the effects related to the dispersive properties of GaAs. In the model, the refractive index is a constant $n = 3.67 + i \cdot 0.03$ with a lower value of intrinsic material absorption in comparison to GaAs. Figure 2(a) shows the simulated absorption spectra for L ranging from 0.5 to 1 as a map, where we mark the MD and ED modes by dashed lines. For $L = 0.5$, the MD and ED modes are centered at 694 nm and 590 nm, respectively. As we gradually increase L, the ED mode gradually shifts by over 200 nm, whereas the MD mode experiences only a small shift. The two modes cross at $L \sim 0.75$–0.8, and the absorption is considerably enhanced at the wavelength of mode crossing, even for the low level of intrinsic absorption used in the simulations. For realistic values of intrinsic absorption in GaAs (Palik model), we find that almost perfect absorption occurs at the wavelength of mode crossing, as shown in Fig. 2(b).

The enhanced absorption at the point of mode crossing confirms that the effect is due to the simultaneous excitation of two modes of opposite symmetry. The close-to-unity absorption in Fig. 2(b), however, occurs only at the wavelength of mode crossing and only for a narrow range of intrinsic material absorption values (see the supplementary material for details). Therefore, we next discuss how the perfect absorption effect can be achieved for different values of intrinsic absorption, specifically in GaAs at different wavelengths near the bandgap edge.

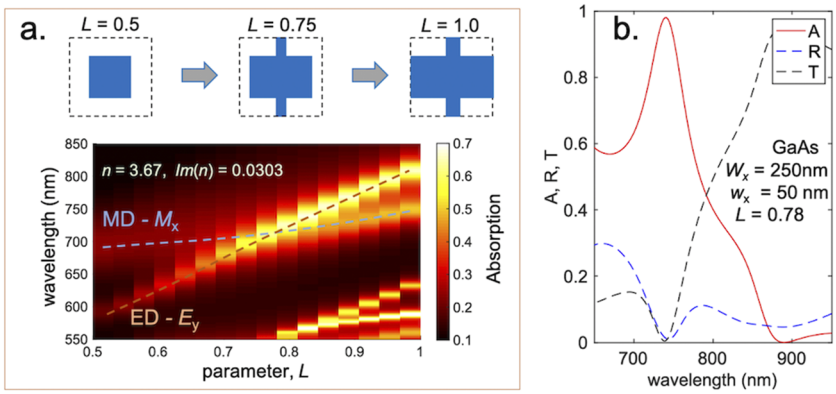

FIG. 2. (a) Tuning of the ED and MD modes under the transformation from the array of cubic resonators to the interconnected resonator network, as shown in the inset. The absorption map is calculated for the case of reduced intrinsic absorption and no dispersion: Re(n) = 3.67 and Im(n) = 0.03 throughout the considered wavelength range. (b) Simulated absorption, reflectivity, and transmission spectra for the $L = 0.78$ case, where the ED and MD modes cross and become degenerate. The Palik model is used to define material properties for the GaAs resonators in (b).

B. Wavelength tuning of the perfect absorption effect

We consider a special case of $L = 1$ for which the resonators positioned along the x-axis are joined into continuous bars. This metasurface design is particularly attractive for optoelectronic applications as it contains conductive channels in both the x- and y-directions [Fig. 1(d)]. First, we note that for the $L = 1$ case in Fig. 2(a), the ED and MD modes are not degenerate. However, using the idea of wavelength tuning through coupling to adjacent resonators,[37–40] we can adjust the wavelengths of the MD and ED modes.

There are only five geometrical parameters fully defining the $L = 1$ metasurface: the width of orthogonal channels, w_x and W_y, the metasurface thickness a, and the periodicities, P_x and P_y [Fig. 1(c)]. Remarkably, we only need to adjust the array periodicity to achieve the ED and MD mode degeneracy. We find that the periodicity along the y-axis affects mainly the MD mode, whereas the x-periodicity affects mainly the ED mode (see the supplementary material for details). Therefore, we achieve mode degeneracy by changing period P_y to 370 nm while keeping period P_x at 320 nm. The mode crossing for these periods occurs at ~760 nm. It is important to note that light with the electric field vector along the narrow channel (y-axis) is required for the excitation of these two modes. Orthogonally polarized light can excite modes with the ED vector parallel to the x-axis and MD vector parallel to the y-axis; however, the latter modes are not degenerate and the metasurface exhibits separate and weaker absorption peaks.

In general, adjusting the array periodicity provides one simple way to achieve and fine-tune the ED and MD mode degeneracy condition for a desired wavelength. Despite small perturbations to their profiles, the ED and MD modes resemble the classical modes for a cubic resonator. Figure 3 illustrates numerically the simulated field profiles for the ED and MD modes for $P_y = 270$ nm and $P_x = 270$ nm.

Having achieved the mode degeneracy, we now describe a practical method for tuning the two modes together and achieving the perfect absorption effect at a desired wavelength. Remarkably, the width of the wider channel W_y affects both modes in a similar manner, and the modes tune together in the wavelength range between 750 nm and 850 nm [Fig. 4(a)]. In fact, it is difficult to resolve one mode from the other in the absorption spectra for the metasurface made of GaAs since the intrinsic absorption broadens both peaks significantly. We can observe the separation of the two modes only for a channel width W_y of less than 100 nm, as shown by the dashed lines in Fig. 4(a). The variation of the wider channel width allows us to tune the two modes from about 750 nm to 850 nm while maintaining the mode degeneracy.

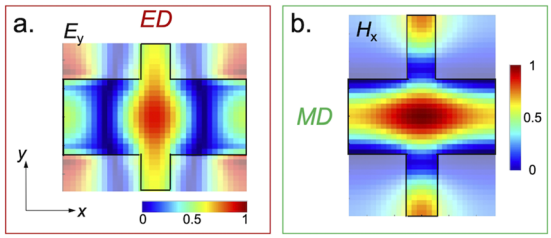

FIG. 3. (a) Electric field distribution (E_y) for the ED mode for $P_x = 320$ nm. (b) Magnetic field distribution (H_x) for the MD mode for $P_y = 370$ nm. Other field components, E_x and E_z for the ED mode, and H_y and H_z for the MD mode, are significantly smaller than E_y and H_x, respectively. To eliminate contributions of the MD mode in (a) and the ED mode in (b), the modes are tuned away to shorter wavelengths by selecting $P_y = 270$ nm in (a) and $P_x = 270$ nm in (b) (see the supplementary material).

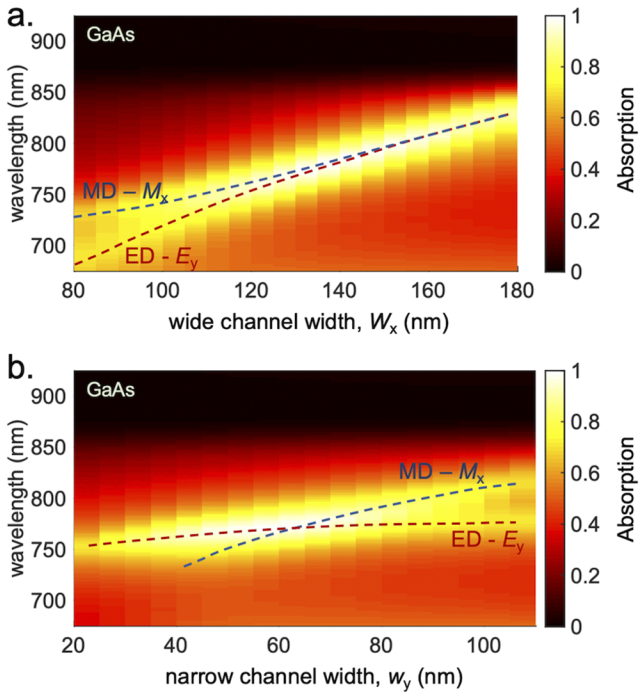

FIG. 4. (a) Tuning of the enhanced absorption wavelength with the wide channel width W_y for the $L = 1$ metasurface with $w_x = 60$ nm, $P_x = 320$ nm, and $P_y = 370$ nm. (b) Adjustment of the critical coupling condition using the narrow channel width w_x for the $L = 1$ metasurface with $W_y = 130$ nm, $P_x = 320$ nm, and $P_y = 370$ nm.

Within this tuning range, the intrinsic absorption in GaAs changes by more than a factor of 2 from strong (at 750 nm) to relatively weak (at 850 nm, near the bandgap edge). The change in intrinsic absorption breaks down the critical coupling condition, i.e., the delicate balance of intrinsic and radiative losses. However, the metasurface design allows us to adjust the balance while keeping the two modes degenerate.

We regain the critical coupling condition by adjusting the width of the narrow channel w_x. The effect of the channel on intrinsic absorption for each mode can be understood if one considers the distribution of the mode energy within the metasurface. For the ED mode, the electric field of the mode is distributed both in the absorbing dielectric and outside of it, in particular around the narrow channel [Fig. 3(a)]. By changing its width, we can force a larger or smaller fraction of the mode energy to interact with the absorbing dielectric and, therefore, increase or reduce the intrinsic mode losses. Similarly, the channel width affects the intrinsic losses for the MD mode [Fig. 3(b)]. Therefore, we can use the narrow channel width as a tuning knob for adjusting the intrinsic mode losses of both modes

while maintaining the mode degeneracy. In Fig. 4(b), we illustrate the effect of the channel width w_x in an absorption map. It shows that the two modes spectrally overlap over a reasonably wide range of widths; however, perfect absorption occurs only near $w_x \sim 60$ nm, highlighting the importance of balancing the intrinsic and radiative losses.

We note that although the narrow channel width slightly affects the mode wavelengths and the mode profiles, this perturbation is not significant. We find that we can use the channel width as the only parameter for adjusting critical coupling successfully for different wavelengths, i.e., for different levels of intrinsic absorption in GaAs, as shown in Sec. II C. For completeness, we briefly comment on the effect of the metasurface thickness a: the variation of the thickness quickly leads to the loss of mode degeneracy, contrary to the effect of the wide channel width. Nevertheless, using the methodology discussed above, perfectly absorbing metasurfaces can be designed for a different thickness of the GaAs layer, for example, $a = 200$ nm.

C. Perfect absorption at selected wavelengths

Now, we find perfectly absorbing metasurface designs for selected wavelengths near the bandgap region of GaAs, from 700 nm to 850 nm. Starting from the $L = 1$ metasurface with $w_x = 60$ nm, $W_y = 130$ nm, and periods $P_x = 320$ nm and $P_y = 370$ nm, which exhibits perfect absorption in the middle of this range (at 775 nm), we tune the two modes to shorter wavelengths (~715 nm) by reducing the wide channel width to $W_y = 100$ nm. With this shift, the maximum absorption decreases at the wavelength of mode crossing, despite a higher value of the material's absorption. Now, by adjusting the narrow channel width to 40 nm, we reduce the intrinsic mode absorption (due to the mode overlap with the material) and restore the critical coupling condition (Fig. 5). Similarly, increasing the wide channel width to 180 nm allows us to shift the two modes to a longer wavelength (~840 nm). Again, the critical coupling condition breaks down with the shift, now, because the material loss is reduced at the longer wavelength. However, by adjusting the narrow channel, we bring the peak absorption back to >99% (Fig. 5). We emphasize that the intrinsic absorption in GaAs varies by more than a factor of 2 within this wavelength range; nevertheless, the flexibility of the proposed metasurface design allows us to achieve perfect absorption throughout this range making this design useful for GaAs devices operating with Ti:sapphire lasers.

To verify that the developed designs resonantly enhance absorption, we fabricate metasurfaces with different channel widths [Fig. 6(a)] and transfer the metasurfaces onto a transparent substrate using optical epoxy ($n = 1.57$) following an electron beam lithography fabrication process described in Ref. 17 (see the supplementary material for details). Transmission spectra of fabricated metasurfaces are measured with a polarized focused beam (NA = 0.16). They show a clear absorption peak at the resonance wavelength in good agreement with numerical simulations. After optimizing the narrow bar width, as outlined above, transmission at the resonant wavelength can be reduced down to the level of 7%–9% [Fig. 6(b)]. As we vary the channel width W_y from 140 nm to 170 nm, the resonance wavelength shifts by ~50 nm toward longer wavelengths, consistent with the simulations in Fig. 4(a). We note that a fabrication tolerance of ~5 nm is required to achieve enhanced absorption at a desired wavelength.

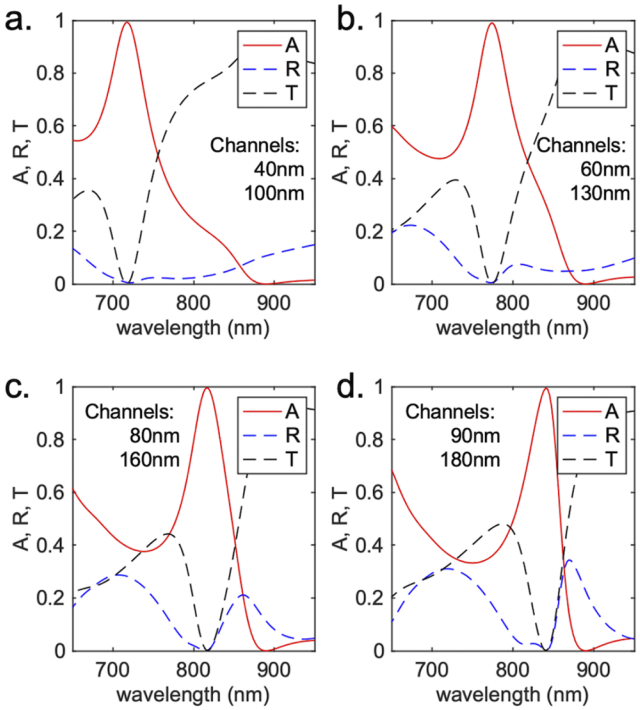

FIG. 5. Absorption, reflectivity, and transmission spectra for four GaAs metasurface designs resulting in perfect absorption at 715 nm (a), 775 nm (b), 815 nm (c), and 840 nm (d).

In the experiment, we find small (7%–9%) residual transmission at the enhanced absorption wavelength. We attribute this deviation from perfect absorption to two factors: (1) imperfections in the metasurface structure and (2) using a focused optical beam for

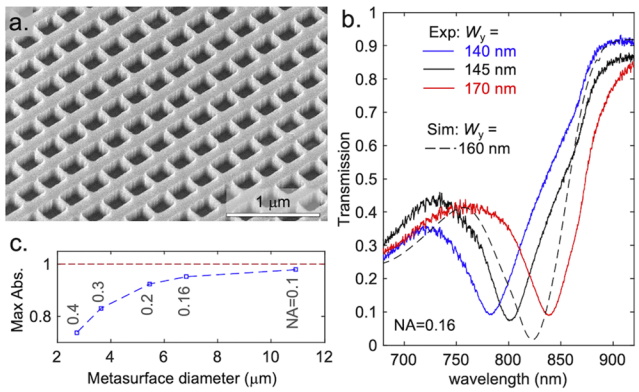

FIG. 6. (a) Scanning electron micrograph (SEM) of metasurfaces with the wide channel width $W_y = 145 \pm 5$ nm estimated using zoomed-in SEM images. (b) Experimental transmission spectra of selected metasurfaces with $W_y = 140$ nm, 145 nm, and 170 ± 5 nm; the narrow channel width is estimated to be 62 nm, 53 nm, and 70 ± 5 nm. The dashed line shows a numerically simulated transmission spectrum for NA = 0.16 for comparison. (c) Maximum simulated absorption for focused Gaussian beams as a function of the metasurface diameter. The labels specify the required numerical aperture (NA) for matching the beam to the metasurface diameter.

testing. The beam is focused by a lens with a numerical aperture (NA) of 0.16, and it contains k-vector components incident on the metasurface at non-zero angles, whereas our simulations assume an infinite metasurface and plane wave illumination. To evaluate the significance of the latter factor, we numerically simulate a finite size metasurface illuminated with Gaussian beams focused with NA = 0.1–0.4. The absorption level for Gaussian beams reduces with the NA. Figure 6(b) illustrates the simulated transmission spectrum for NA = 0.16 with small residual transmission, confirming the experimental spectra.

The impact of beam focusing is important for practical applications of these metasurfaces, and below, we estimate this impact on the perfect absorption effect. For each simulated Gaussian beam, we determine the diameter of the area that receives 99% of the incident power (λ = 800 nm), and in Fig. 6(c), we plot the maximum absorbed power by that area as a function of that diameter. This level of absorption can be achieved if the Gaussian beam size is matched to the metasurface size, and such matching can be realized by selecting a lens with NA values shown in Fig. 6(c). For example, for NA = 0.16 and a metasurface of 6.8 μm in diameter, the maximum of ~95% can be absorbed, whereas a 11 μm diameter metasurface can absorb the maximum of ~98% with NA = 0.1.

D. Perfectly absorbing metasurface applications

Finally, we illustrate the potential applications of optoelectronic devices, where a bulk semiconducting element can be replaced with a thin perfectly absorbing metasurface to improve the device efficiency and performance. As a first example, Fig. 7(a) illustrates a photoconductive switch with a GaAs metasurface for THz detection and generation,[32] where the in-plane conductivity can be efficiently switched between the ON and OFF states with laser light at the wavelength of perfect absorption. The metasurface provides the complete absorption of incident photons of the gating pulse, eliminating significant reflection losses and the need for a thicker absorbing region (typically 1 μm–2 μm), while improving the contrast in conductivity between the ON and OFF states. In a second example, Fig. 7(b) illustrates a PIN photodiode,[43] where an InGaAs metasurface can serve as an efficient absorber and simultaneously as the vertical charge transport channel. As in the first example, the metasurface provides the efficient absorption of incident photons and elimination of reflection losses. Furthermore, it reduces the distance between the p-doped and n-doped regions, leading to a smaller voltage bias required for PIN photodiode operation and a shorter charge carrier transient time. Finally, the use of narrow channels for current conduction instead of bulk material also leads to lower dark current noise.

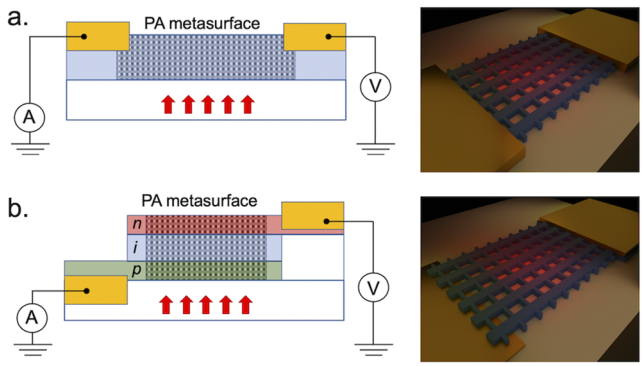

FIG. 7. Schematic diagrams of the perfectly absorbing metasurface in a photoconductive switch (a) and in a PIN photodiode (b).

III. CONCLUSION

In summary, we propose and numerically demonstrate an all-dielectric perfectly absorbing metasurface consisting of rectangular resonators with electrical conduction channels. We use the channels not only for enabling optoelectronic applications but also for effective adjustment of the critical coupling condition at different wavelengths of operation and different levels of intrinsic material absorption. To facilitate an intuitive understanding of the design, we reveal the underlying physics of perfect absorption and describe the effects of geometrical parameters on the ED and MD modes. As a result, the metasurface geometry can be adjusted in order to satisfy all three essential conditions for the perfect absorption effect: modes degeneracy, mode symmetry, and critical coupling for a desired wavelength of operation. In particular, we design GaAs metasurfaces for operation wavelengths ranging from 715 nm to 840 nm, the spectral region with large variation in the intrinsic absorption level in GaAs. We also experimentally confirm that such metasurfaces resonantly enhance optical absorption. This work opens doors for a new generation of efficient optoelectronic devices with integrated optical metasurfaces, as this design offers possibilities to engineer not only the optical but also electronic properties and improve the efficiency of photodetectors while reducing the active material thickness.

SUPPLEMENTARY MATERIAL

See the supplementary material for metasurface fabrication and numerical simulation details and results showing the effect of critical coupling on maximum absorption at the point of mode crossing for the ED and MD modes (Fig. S1), the effect of inter-resonator coupling on the ED and MD modes (Fig. S2), and the effect of metasurface thickness on the ED and MD modes (Fig. S3).

AUTHORS' CONTRIBUTIONS

O.M. and L.H. performed numerical simulations. O.M., S.J.A., and J.L.R. fabricated metasurface samples. All authors contributed to the metasurface design development, the analysis of the results, and the manuscript editing.

ACKNOWLEDGMENTS

This work was supported by the U.S. Department of Energy, Office of Basic Energy Sciences, Division of Materials Sciences and Engineering and performed, in part, at the Center for Integrated Nanotechnologies, an Office of Science User Facility operated for

the U.S. Department of Energy, Office of Science. Sandia National Laboratories is a multimission laboratory managed and operated by National Technology and Engineering Solutions of Sandia, LLC, a wholly owned subsidiary of Honeywell International, Inc., for the U.S. Department of Energy's National Nuclear Security Administration under Contract No. DE-NA0003525. This paper describes objective technical results and analysis. Any subjective views or opinions that might be expressed in the paper do not necessarily represent the views of the U.S. Department of Energy or the United States Government. O.M. and L.H. acknowledge the support of the EPSRC (Grant Nos. EP/P021859/1 and EP/L015455/1).

DATA AVAILABILITY

The data that support the findings of this study are available from the corresponding author upon reasonable request.

REFERENCES

[1] I. Brener, S. Liu, I. Staude, J. Valentine, and C. L. Holloway, *Dielectric Metamaterials: Fundamentals, Designs and Applications*, 1st ed. (Woodhead Publishing, 2019).
[2] D. Neshev and I. Aharonovich, Light: Sci. Appl. **7**, 58 (2018).
[3] K. Fan *et al.*, Adv. Mater. **30**, 1800278 (2018).
[4] S. M. Kamali *et al.*, Nanophotonics **7**(6), 1041 (2018).
[5] A. M. Shaltout *et al.*, Science **364**(6441), eaat3100 (2019).
[6] P. Genevet *et al.*, Optica **4**(1), 139 (2017).
[7] N. Yu *et al.*, Nat. Mater. **13**, 139 (2014).
[8] N. Yu *et al.*, Science **334**(6054), 333 (2011).
[9] M. Decker *et al.*, Adv. Opt. Mater. **3**(6), 813 (2015).
[10] A. K. Azad *et al.*, Sci. Rep. **6**, 20347 (2016).
[11] C.-C. Chang *et al.*, Nano Lett. **18**(12), 7665 (2018).
[12] J.-Y. Jung *et al.*, Sci. Rep. **7**, 430 (2017).
[13] X. Xu *et al.*, Nano Lett. **18**(6), 3362 (2018).
[14] M. D. Goldflam *et al.*, Appl. Phys. Lett. **109**, 251103 (2016).
[15] M. D. Goldflam *et al.*, Opt. Express **25**, 12400 (2017).
[16] O. Mitrofanov *et al.*, APL Photonics **3**(3), 051703 (2018).
[17] T. Siday *et al.*, Nano Lett. **19**, 2888 (2019).
[18] Y. Ra'di *et al.*, Phys. Rev. Appl. **3**, 037001 (2015).
[19] P. Yu *et al.*, Adv. Opt. Mater. **7**, 1800995 (2019).
[20] M. A. Kats and F. Capasso, Laser Photonics Rev. **10**(5), 735 (2016).
[21] N. Liu *et al.*, Nano Lett. **10**, 2342 (2010).
[22] C. M. Watts *et al.*, Adv. Mater. **24**, OP98 (2012).
[23] H.-T. Chen, Opt. Express **20**, 7165 (2012).
[24] S. Kim *et al.*, Nano Lett. **18**(2), 971 (2018).
[25] X. Zhao *et al.*, ACS Photonics **6**, 830 (2019).
[26] J. R. Piper and S. Fan, ACS Photonics **1**, 347 (2014).
[27] H. Zhou *et al.*, Optica **3**(10), 1079 (2016).
[28] B. C. P. Strumberg *et al.*, Optica **3**(6), 556–562 (2016).
[29] M. A. Cole *et al.*, Nanotechnology **27**, 424003 (2016).
[30] X. Ming *et al.*, Opt. Express **25**(20), 24658 (2017).
[31] J. Tian *et al.*, ACS Photonics **7**(6), 1436–1443 (2020).
[32] O. Mitrofanov and I. Brener, Photoniques **101**, 47–52 (2020).
[33] J. R. Piper *et al.*, Appl. Phys. Lett. **104**(25), 251110 (2014).
[34] A. Cardin *et al.*, Opt. Express **26**, 17669 (2018).
[35] A. I. Kuznetsov *et al.*, Science **354**(6314), aag2472 (2016).
[36] M. Kerker *et al.*, J. Opt. Soc. Am. **73**(6), 765–767 (1983).
[37] K. E. Chong *et al.*, ACS Photonics **3**(4), 514 (2016).
[38] K. E. Chong *et al.*, Nano Lett. **15**(8), 5369 (2015).
[39] V. E. Babicheva and A. B. Evlyukhin, Laser Photonics Rev. **11**, 1700132 (2017).
[40] C.-Y. Yang *et al.*, ACS Photonics **5**, 2596 (2018).
[41] Q. Yang *et al.*, Adv. Funct. Mater. **30**, 1906851 (2020).
[42] See http://www.lumerical.com/tcad-products/fdtd/ for Lumerical, Inc.
[43] A. Beling and J. C. Campbell, J. Lightwave Technol. **27**, 343 (2009).